SAND2022-4915J

STUDY OF ALKALINE CARBONATE COOLING TO MITIGATE EX-VESSEL MOLTEN CORIUM ACCIDENTS

David L.Y. Louie, Yifeng Wang, Rekha Rao, Alec Kucala and Jessica Kruichak
Sandia National Laboratories
1515 Eubank SE, Albuquerque, NM 87123, U.S.A.
dllouie@sandia.gov ; ywang@sandia.gov; rrrao@sandia.gov; akucala@sandia.gov; jnkruic@sandia.gov

Highlights

- Heat absorption from carbonate mineral decomposition can be used to quickly solidify molten corium and mitigate a nuclear reactor accident.
- This concept can be implemented with an injectable granular material suitable for integration into an existing nuclear power plant accident management system.
- MELCOR, a severe nuclear accident analysis code, was used to demonstrate the effectiveness of the novel injectable mitigation system in a simulated reactor accident.
- The MELCOR analysis demonstrates that using this carbonate injection system can delay the destructive hydrogen explosion by more than 17 hours, which is sufficient for the accident management team to further moderate the accident.

ABSTRACT

To mitigate adverse effects from molten corium following a reactor pressure vessel failure (RPVF), some new reactor designs employ a core catcher and a sacrificial material (SM), such as ceramic or concrete, to stabilize the molten corium and avoid containment breach. Existing reactors cannot easily be modified to include these SMs but could be modified to allow injectable cooling materials. Current reactor designs are limited to using water to stabilize the corium, but this can create other issues such as reaction of water with the concrete forming hydrogen gas. The novel SM proposed here is a granular carbonate mineral that can be used in existing light water reactor plants. The granular carbonate will decompose when exposed to heat, inducing an endothermic reaction to quickly solidify the corium in place and producing a mineral oxide and carbon dioxide. Corium spreading is a complex process strongly influenced by coupled chemical reactions, including decay heat from the corium, phase change, and reactions between the concrete containment and available water. A recently completed Sandia National Laboratories laboratory directed research and development (LDRD) project focused on two research areas: experiments to demonstrate the feasibility of the novel SM concept, and modeling activities to determine the potential applications of the concept to actual nuclear plants. Small-scale experiments using lead oxide (PbO) as a surrogate for molten corium demonstrate that the reaction of the SM with molten PbO results in a fast solidification of the melt due to the endothermic carbonate decomposition reaction and the formation of open pore structures in the solidified PbO from CO_2 released during the decomposition. A simplified carbonate decomposition model was developed to predict thermal decomposition of carbonate mineral in contact with corium. This model was incorporated into MELCOR, a severe accident nuclear reactor code. A full-plant MELCOR simulation suggests that by the introduction of SM to the reactor cavity prior to RPVF ex-vessel accident progression, e.g.,

core-concrete interaction and core spreading on the containment floor, could be delayed by at least 15 hours; this may be enough for additional accident management to be implemented to alleviate the situation.

KEYWORDS
Nuclear accident, molten corium, mitigation, MELCOR, corium spreading

1. INTRODUCTION

The last major nuclear accident, Fukushima Daichi, caused significant financial burdens, detrimental environmental impacts, and damage to public confidence about the importance of nuclear power as part of a diversified energy portfolio. Effective accident mitigation strategies are essential to both bolster public support and reduce the potential impact of nuclear accidents to the environment. In a core meltdown, such as at Fukushima, the subsequent reactor pressure vessel (RPV) failure could lead to a molten corium release to the drywell in a boiling water reactor (BWR) (Figure 1). The molten corium released could further spread out to the wet well and breach the containment. Hydrogen production from corium interactions with water and concrete could also cause an explosion and further environmental contamination by releasing radioactive fission products. In the last few decades, several experiments have been performed to investigate the corium spreading and cooling in the cavity region below the RPV, where significant corium interactions with concrete and water can occur [1-3]. These experiments were conducted to determine how corium spreads while reacting with the substrate such as concrete and water. To better understand these experiments, several analytical models and computer codes were developed to simulate the corium spreading and reacting [4-13]. Future reactor designs must include engineered safety systems to minimize corium flow and ensure effective cooling, immobilization of the core melt, elimination or minimization of hydrogen gas production, and maximization of radionuclide retention. Employment of a core catcher and slab sacrificial material (SM), such as ceramic and concrete slab, to slow the corium flow have been incorporated into many new reactor designs [14-16]. Because existing operating light water reactors (LWRs) cannot easily be modified to include a core catcher or these SMs, an injectable mitigation system (IMS) using a granular SM could be implemented without major retrofits.

A laboratory directed research development (LDRD) research project was conducted at Sandia National Laboratories (SNL) to investigate the feasibility of developing an IMS using granular carbonate materials. Mineral carbonates thermally decompose and absorb energy (Table 1), thus providing cooling to quickly solidify molten corium. Table 1 provides energy absorption values for carbonate minerals and water for comparison. As shown, carbonate materials have a higher energy absorption value than on a water per mole and volume basis. Because water is a primary coolant in the LWRs, the co-existence of water and carbonate minerals needs to be addressed if a carbonate mineral is deployed to mitigate reactor accidents. The use of commonly found alkaline carbonates is inexpensive since much of these carbonates exist in nature in large quantities; however, the cost associated for grinding them into granules need to be considered. Many of the alkaline oxides are reactive with water forming alkaline hydroxide in a reversible reaction which is not a concern [17-24].

The focus of this research is to demonstrate the feasibility of using a granular carbonate IMS to contain and cool ex-vessel molten corium [17]. This is demonstrated here using a series of surrogate experiments, the finite-element (FEM) software Sierra/Aria, and MELCOR. Sierra/Aria was developed at SNL to solve complex multiphysics problems and was used to simulate molten corium spreading experiments as reported in a previous paper [25]. MELCOR is a U.S. Nuclear Regulatory Commission severe accident code developed at SNL [26] and is used here to model the corium/concrete interaction in the reactor cavity [27].

In this paper, we show how a SM with high energy absorption rates can be used to reduce the spreading rate of corium, presenting a possible solution for accident management during a reactor meltdown. In Section 2.1, we will demonstrate how this SM behaves in bench-scale experiments using lead oxide (PbO) as a surrogate for corium, as well as in larger surrogate tests in Section 2.2. As we scale up to the plant-scale using MELCOR, a shrinking-core model will be used to model the endothermic reaction of SM particles with the spreading corium. This is described in Section 3. In Section 4, we use MELCOR to model the FARO L-26S experiment and predict the corium spreading rate with and without granular calcium carbonate. These results can be compared to the experimental data and the results obtained from FEM simulations using Sierra/Aria. Section 5 use MELCOR on a Mark I reactor accident and shows the effect of using a calcium carbonate SM. Finally, in Section 6, we end with some concluding remarks and ideas for the next steps in the research.

2. EXPERIMENTS

Small-scale (grams) and large-scale (kilograms) experiments were conducted using PbO as a surrogate for corium melt, since PbO is readily available and has a high density (similar to UO_2) and a melting point just slightly higher than the $CaCO_3$ decomposition temperature of 825 ºC.

2.1 Small-Scale Tests

For proof of the concept, over 30 sets of benchtop SM-melt interaction experiments were conducted with various carbonate SMs (i.e., calcite, dolomites) and PbO melt masses [17]. SM-melt experiments consist of molten PbO poured onto a petri dish filled with a carbonate mineral (MCO_3). In each test, a certain quantity of PbO was first melted at ~ 1250 K. The melt was then poured into a silica dish containing a known amount of MCO_3. The temperature change and the extent of melt solidification were monitored in real-time using a remote temperature gun and a video camera. Post-experimental tests were also performed to determine microstructures, chemical composition variations, and CO_2 bubble distributions in the resulting solidified materials.

The tests clearly indicate multi-scale bubble formations in the solidified materials (Figures 2-4). Weight measurements were conducted to estimate the loss of carbon dioxide from carbonate being decomposed as a function of the interacted PbO mass. Due to the release and trapping of CO_2 during the reactions, a water volume measurement was done on selected samples to determine the porosity of the open pore structure. In addition, we conducted a number of thermo-gravimetrical analyses (TGAs) for the samples of carbonates. For example, we measured a decomposition energy for $CaCO_3$ powder of 194 kJ/mole [17].

To minimize heat loss to the surroundings, tests were conducted in a petri dish preheated at 823 K, in which molten PbO at 1248 K was poured onto a layer of $CaCO_3$ powder. The result of this

experiment is shown in Figure 2, which shows that the now solidified sample has an open porous structure with a large void at the top. The porosity of the solidified lead oxide was measured using a water displacement technique to calculate the bulk density, which in turn was used to estimate the bulk porosity of the material. Since some decomposition products (CaO) may be trapped in the sample, the bulk porosity was estimated to be as high as 70% [17].

The results of a similar test without preheating are shown in Figure 3. As shown in Figure 3(a), the swelling is observed due to build-up of CO_2 through the melt while it is solidifying. The distributions of micron-sized bubbles are shown in Figure 3 (b) to (d). As shown in Figure 3(b), the bubbles are concentrated near the surface of the sample, which suggests a convective flow along the surface during solidification resulting in larger bubbles concentrating near the top of the sample. This allows open pores to develop near the top of the surface of the sample as evidenced in Figure 3(b). Another test with dolomite is shown in Figure 4, where a similar open pore structure is observed along with a distribution of unreacted dolomite on the surface of the sample, possibly indicating strong convective flow caused by the reaction. Note that these observations of porous structures are similar to those observed in the COMET spreading experiment [28], where some convective flows were seen based on the bubble distribution within the sample.

2.2. Large-Scale Tests

To verify scalability from the small-scale tests as described earlier, several large-scale confirmatory tests were performed using approximately 1 kilogram of PbO. To conduct this larger test, we used a tube furnace with a containment tube made of alumina. A crucible tube was also used to hold and pour the molten PbO onto the catch pan which contained the MCO_3 or other test materials. In Figure 5, we show the apparatus used for the large-scale tests, where the tube furnace is mounted on a crank shaft. This hand crank is used to slowly pour the molten PbO onto the sacrificial material. The tube is pointed upward, as shown in this figure, while the PbO is melting inside the heating tube. When the melt reaches a desired liquid temperature (approximately 1273 K), the crank shaft is turned to pour the PbO melt into the catch pan where a sand or carbonate bed is located. Several thermocouples are added to monitor the temperature in the pan and in the air around the furnace.

The large-scale pour tests further confirm the experimental results obtained from the small-scale tests; we see that the endothermic decomposition of alkaline carbonate mineral can effectively remove heat from molten PbO leading to quick solidification of the melt. Similar to the small-scale experiments, the solidified PbO is shown to have multiple-scale pores from the CO_2 gas released from carbonate decomposition (Figure 6). Vigorous convection and mixing were also observed. The convection and mixing were driven by the density inversion in the system as well as by CO_2 buoyancy and degassing.

3. SHRINKING CORE MODEL

In order to account for the endothermic reaction of the sacrificial material in MELCOR, a simplified shrinking core model (SCM) [19-24] was developed [17]. The decomposition reaction of an alkaline carbonate is given below:

$$\mathbf{MCO_3} + \Delta\mathbf{H} \xrightarrow{\mathcal{R}} \mathbf{MO} + \mathbf{CO_2(g)} \qquad (1)$$

where $\mathcal{R}$ is the reaction rate in mole/m^2-s, and ΔH is the endothermic reaction energy in J/mole. For $CaCO_3$, ΔH has a range of 178 to 182kJ/mol [18, 22], including our TGA measured value of 194 kJ/mol. In this research we assume ΔH of 182.1 kJ/mol. $\mathcal{R}$ in Equation (1) is given by:

$$\boldsymbol{\mathcal{R} = k(P_e - P)} \tag{2}$$

where k is the reaction rate constant (mol/m^2-s-Pa), $P_e$is the equilibrium pressure of CO_2 and P is the pressure at the unreacted MCO_3 surface. Both k and P_e are given as:

$$\boldsymbol{k = k_0 e^{-\frac{\Delta E_R}{RT}}} \tag{3}$$

$$\boldsymbol{P_e = P_e^0 e^{-\frac{\Delta H}{RT}}} \tag{4}$$

where $\boldsymbol{k_0}$ **is** $\boldsymbol{1.22 \times 10^{-5}}$ mole/m^2-s-Pa, $\boldsymbol{\Delta E_R}$ is the activation energy, 33472.16 J/mole [22] and $\boldsymbol{P_e^0}$ **equals to** $\boldsymbol{2.15 \times 10^7}$ atm for $CaCO_3$. R in the above equations is the gas constant (8.314 J/mole-K or Pa m^3/mol-K), T is the temperature of the carbonate (K). Figure 7 shows a schematic of a simplified SCM for the carbonate sphere-corium interaction, where the sphere is in the range of few millimeters to centimeters being decomposed as it absorbs the heat from the surrounding corium melt. In this model, we assume a quasi-steady state condition.

Figure 7 shows the shrinking radius of r for the carbonate sphere, which has an initial radius of r_0. The decomposed region between r and r_0 represents a porous region where the MO pores are occupied with CO_2 gas. The boundary temperature is represented by the melt temperature (T_m) and its corresponding gas pressure (P_m). Solving the differential equation for a sphere, the temperature of the unreacted core, T as shown in Figure 12 is given by:

$$T = T_m - \frac{\mathcal{R}\cdot\Delta H\cdot r}{\lambda}\left(1 - \frac{r}{r_0}\right). \tag{5}$$

Let m equal the mass of $CaCO_3$ remaining, and m_0 is the initial mass of $CaCO_3$, then define f equals to $\frac{m}{m_0}$. Assuming a spherical shape for the particle, f can be redefined in terms of the initial and evolving radius of the spherical particle: f is defined as $\left(\frac{r}{r_0}\right)^3$. Now Eq. (5) can be rewritten as in terms of f:

$$T = T_m - \frac{\mathcal{R}\cdot\Delta H\cdot r_0 f^{1/3}}{\lambda}\left(1 - f^{1/3}\right) \tag{6}$$

Since the CO_2 generated from the decomposition diffuses through the outer porous oxide region, MO, via the gas pressure gradient. This diffusion, D, is given by:

$$D = D_0 e^{\alpha T_s} \tag{7}$$

where α is given as 0.0165 K^{-1} [22], $D_0$is given as 8.36×10^{-6}m^2/s at 830 °C [23]. This is for the $CaCO_3$ decomposition. T_s in Eq. (7) is the temperature in the oxide region of the sphere defined between r_0 to r, as shown in Figure 4.

$$T_s = T_m - \frac{\mathcal{R}\cdot\Delta H\cdot r_0}{\lambda}\left(\frac{1+f^{1/3}}{2} - \frac{f^{2/3}+f^{1/3}+1}{3}\right) \tag{8}$$

Thus, this diffusion could affect the pressure at the surface of the unreacted sphere, P. The pressure, P, can be determined from the temperature, f, and the pressure in the corium:

$$P = P_m + \frac{R \cdot T \cdot \mathcal{R} \cdot r_0 f^{1/3}}{D}\left(1 - f^{1/3}\right) \quad (9)$$

where T_m and P_m are the temperature and pressure of the corium melt.

The heat removal rate as the surface of the MCO_3 sphere reacts is given by:

$$\dot{q}_{heat} = 4\pi r^2 \mathcal{R} \cdot \Delta H \quad (10)$$

Reaction product such as CO_2 and MO in terms of mole/s, $\dot{M}_{prod}$ from the decomposition of MCO_3 is given by:

$$\dot{M}_{prod} = 4\pi r^2 \mathcal{R} \quad (11)$$

So far, we have derived the equations for a single sphere of MCO_3 thermal decomposition due to the surrounding melt. To consider the entire bed of carbonate spheres surrounded by melt using the single sphere model, several assumptions were made:

1. Each sphere is surrounded by the melt,
2. Each sphere has the same size,
3. Each sphere will absorb the same energy from the melt,
4. The bed has a constant porosity, and
5. Edge effects are ignored.

In a carbonate bed with a porosity (ε), 1- ε is the volume occupied by all spheres, ϕ. The mass consumption rate is given by:

$$\frac{dm}{dt} = -\phi \nu_{MCO_3} \mathcal{R} \cdot \frac{3f^{2/3}}{r_0} m_0 \quad (12)$$

Both heat loss and CO_2 generation (moles) can be given by:

$$\frac{dQ_{heat}}{dt} = \frac{dm}{dt}\left(\frac{\Delta H}{\mathcal{M}} + C_{p_{MCO_3}}(T - T_0)\right) \quad (13)$$

$$\frac{dM_{CO_2}}{dt} = -\frac{1}{\mathcal{M}}\frac{dm}{dt} \quad (14)$$

Eq. (13) also includes the sensible heat for the reacting materials, where $C_{p_{MCO_3}}$ is the heat capacity for MCO_3 (1251.02 J/kg-K at 1000 K for $CaCO_3$ [17]). Note that the rate change of the mole of CO_2 released (M_{CO_2}) is from the decomposition of MCO_3.

4. FARO L-26S STUDY

Before we implemented the SCM into a severe accident model using MELCOR, we wanted to test the functionality of the derived SCM described in the previous section. To do that, we used the FARO corium spreading experiment L-26S. A detailed description of this experiment is given in [29] with the modeling approach discussed in [17]. The schematic of the FARO experiment is shown in Figure 8. Figure 9 shows the spreading plate geometry. The experimental data and the results are given in Tables 2 and 3, respectively. In this paper, we use results from the finite-element code Sierra/Aria [25] to validate the pancake spreading model used in MELCOR.

4.1. Finite Element Method (SIERRA/Aria)

Sierra/Aria is a finite-element code developed at SNL used to solve complex multiphysics problems involving heat transfer and fluid motion. Sierra/Aria was used to model the FARO L-26S study [25] and showed good agreement with the experimental results. In this study, we simulated the advancement of corium melt on a cool steel plate. To model the solidification of the corium, we used a pseudo-solidification model for the viscosity, known as the Ramacciotti model, which bounds the viscosity between a liquid and solid state using the temperature of the material. To capture the corium/air interface, the conformal decomposition finite-element method (CDFEM) [25] was employed which allows for the application of boundary conditions on this interface, including surface tension and convective/radiative heat transfer losses. Overall, the comparison between the simulation and experiments were quite good and demonstrated the applicability of Sierra/Aria to simulate corium spreading scenarios. This simulation will serve as a benchmark to validate the MELCOR spreading model to be outlined in the next section.

4.2. MELCOR

A validation test was conducted to investigate how MELCOR's spreading model corresponded to the FARO L-26S experimental configuration. MELCOR uses a pancake spreading model that does not model any friction on the walls of the spreading plate, shown in Figure 9. The detailed description of the comparison/validation for this experiment is given in [17]. Here, we present a comparison of the MELCOR results with both the experiment and Sierra/Aria modeling effort, briefly described in Section 4.1. In this comparison, we utilize the experimental data to construct the MELCOR model. Note that because the corium spreading model in MELCOR is only a pancake model, the equivalent spreading distance is recalculated based on the geometry of the FARO L-26S experiment shown in Figure 9.

Figure 10 shows the comparison between MELCOR, Sierra/Aria and the experimental data. As shown in Figure 10, the spreading from MELCOR is initially faster than both the experimental data and the Aria results. As mentioned before, MELCOR employs a pancake model and cannot model the channel geometry where wall friction may be significant. The fast-initial spreading in MELCOR may be due to the heat loss to the plate, which takes some time to occur. Once heat loss to the plate and the surrounding environment is sufficient, the rate of spreading is drastically reduced ($t > 3$ s). While the MELCOR results do not closely match the time-history of the corium front location with the experiment and Aria results, the final location of the corium front is in excellent agreement with the benchmark.

In MELCOR, to model the cases where SM is present, two equations are required; the amount of heat being absorbed by the SM and the amount of the CO_2 being generated, described in Equations. (13) and (14), respectively. Equation (13) is used to recompute the melt temperature, T_m where heat in the melt is absorbed by the carbonate decomposition. Eq. (14) is used to compute P_m, since CO_2 gas generation from the endothermic reaction will contribute to the melt pressure. Table 5 shows the sequence of the calculations used. The intent is to extend the derivation of a single carbonate particle's heat and mass transfer to a carbonate bed that consists of a large quantity of uniformly sized carbonate particles.

Instead of hardwiring the SCM model in MELCOR, we decided to implement it as an input model where the model can be written as a series of input records. [17]. Based on the absorption value in Table I, we estimate that about 90 kgs of $CaCO_3$ is needed to stop the spreading faster than the experiment value without any sacrificial material. We assume that the carbonate is fixed to the plate and does not move along with the melt.

In Table 4, we list the several cases from a sensitivity study on the effects of carbonate properties such as size, porosity, and thermal conductivity from the SCM, including a base case with no carbonate (as the MELCOR simulation shown in Figure 10). The calculated spread lengths are provided in the last column of the table. Detailed discussions on the parameters $(\varepsilon, \lambda, \alpha)$ are presented in [17]. Figure 11 shows that the spreading distance increases as the carbonate particle size increases, which is consistent with the fact that smaller particles have higher surface areas per volume. This is also consistent with the amount of the carbonate being consumed as shown in Figure 12(a). The initial slope of the reacted mass seems to be very high, which may not be realistic when the melt first contacts the carbonate. The limiting situation could be that the CO_2 generation may blanket the carbonate particle and reduce the reaction rate, something which may not be captured well in the derivation of the SCM. Because of the large initial reaction rate when the melt contacts the carbonate, the higher CO_2 generation increases the chamber pressure substantially as shown in Figure 12(b). In addition to the particle size effect, we also studied the effect of the thermal conductivity of oxide, gas diffusion coefficient, and porosity of the carbonate and their results are shown in Table 4. Also shown in Table 4, the effects on these parameters are minimal in comparison to particle sizes, which is the most important variable. See [17] for a more detailed discussion of this sensitivity study.

This L-26S MELCOR simulation, with the SCM implementation for the sacrificial material, shows that the endothermic decomposition of carbonate has sufficient energy absorption to quickly cool and solidify the corium. This was measured as a reduction in the over-all spreading distance compared to the base case, a scenario where no sacrificial material was present on the substrate. In the next section, we apply this SCM to the full plant simulation. This application would be used to demonstrate the effectiveness of granular carbonate to mitigate a severe accident scenario.

5. MARK I BWR STUDY

To investigate the potential benefits of introducing the granular carbonate SM to the reactor cavity/pedestal area in a severe nuclear reactor accident, two MELCOR calculations were performed. We used a BWR-4 MELCOR deck for the scenarios. The accident scenario was a long-term station blackout (LTSBO) affecting the BWR-4 reactor situated in a Mark I containment. This is the base case, without the carbonate sacrificial materials. The second calculation was made by adding a large quantity of carbonate materials (using $CaCO_3$) as a SM into the pedestal (drywell) region below the RPV as a postulated scenario to study the change of the accident sequence (see Figure 13). In this second calculation, the SCM was used to model the endothermic reactions that would take place between the molten core debris and $CaCO_3$ on the containment floor. In this scenario, the SM was introduced to the floor area prior to failure of the RPV lower head. The parameters used in the SCM are identical to Case 1 of the FARO L26S simulations in Table 4, except 280 metric tons of $CaCO_3$ were placed onto the pedestal before RPV lower failure (see Figure 13). Based on the analysis [17], the filling time for this mass is on the order of < 3 hours

for a 15.2 cm (6") diameter of the screw type conveyer system. A 33 cm (13 inch) diameter system would reduce the filling time by five times.

To illustrate the accident sequences of these two cases, an event table was constructed and shown in Table 5. The sequence of events for the cases with and without SM injection is the same up to the point when the RPV fails to allow molten corium to relocate onto the pedestal floor below the RPV. The events leading up to RPV failure are described in [17]. Here, we only discuss the comparison between these two cases and show the effectiveness of carbonate cooling to mitigate the accident.

Figure 14 compares the containment pressure with and without sacrificial material. This large difference in containment pressure can be attributed to the core debris spreading on the containment floor to the drywell liner and melting through the liner much earlier in the calculation where no sacrificial material is present. The containment depressurizes through the breach in the liner. It is important to realize that in considering the pressure response in the calculations, the leakage at the drywell head flange is modeled, and that the leakage effectively regulates maximum pressure. Figure 15(a) and Figure 15(b) show partial pressures in the calculations for the base case and with the addition of the decomposing $CaCO_3$ SM. The first noteworthy difference in these figures is that the greater CO_2 pressure develops after core debris first relocates to the containment floor. The second noteworthy difference is the delayed elevation of CO_2 and H_2 pressures in the calculation with the sacrificial material. The higher CO_2 pressure results from the $CaCO_3$ decomposition, while the delayed increase of CO_2 and H_2 pressures reflects delayed core-concrete interaction from the vitrification of the corium flow associated with the endothermicity of the $CaCO_3$ reaction. Note that these comparisons are made only for little over an hour, due to the fact that in the simulation without sacrificial material, melt-through of the drywell liner is observed.

Figure 16(a) shows the temperature of the core debris in the reactor pedestal (on the containment floor beneath the reactor). The cooling of the melt due to the endothermic reaction of $CaCO_3$ with the corium is clearly seen in this figure. Note that the peak temperatures in both cases are due to the concrete ablation. Evidence of the melt cooling is also shown in the decreased pedestal volume temperatures in Figure 16(b) when the SM is present.

Figure 17(a) shows the time histories of the volume of concrete ablated in the two calculations. The histories are quite similar albeit shifted in time. $CaCO_3$ cooling of the melt is responsible for the shift; the cooling causes a substantial delay (15 hours) in the onset of core-concrete interaction. This interaction only occurs after all the SM has been exhausted. Shown in Figure 17(b) is the overall gas generation resulting from both the core-concrete interaction and $CaCO_3$ decomposition. The traces of molecules in this figure includes CO_2, H_2 and water vapor. Gas production is substantially larger in the calculation with $CaCO_3$ decomposition, since the sacrificial material works by absorbing heat and producing carbon dioxide upon heating above the decomposition temperature. The larger gas production would have resulted in substantially higher containment pressure had the reactor head flange not leaked, but the carbon dioxide would not lead to an explosive reaction similar to what occurred with hydrogen at Fukushima since carbon dioxide is already oxidized and will not combust like hydrogen.

Spreading of core debris across the containment floor from the pedestal region beneath the reactor and out the doorway toward the drywell liner (see arrows of the debris flow) is presented in Figure

18. Both calculations show debris reaching the liner but at substantially different times. Debris reaching the liner was assumed to melt through the liner in the MELCOR model, breaching containment. Containment then blew down into the reactor building. The blowdown caused the H_2 concentration to spike in the building as shown in Figure 19(a) and to reach a burnable concentration (0.10 molar fraction H_2). The H_2 ignited, implying gross building damage. (Note that the H_2 in Figure 19(a) does not reach a burnable value only because the time between points comprising the traces is too long to resolve the spikes.)

Figure 19(b) shows a comparison of the molar concentration of H_2 produced in the MELCOR calculations relative to all gas produced from in-vessel oxidation, core-concrete interaction and $CaCO_3$ decomposition. The figure suggests that $CaCO_3$ decomposition in a severe accident could reduce relative H_2 concentration and thereby effectively reduce H_2 ignition potential.

6. CONCLUSIONS

In this paper, we explored the concept of using alkaline carbonate as a SM, in an injectable particulate form, to mitigate the ex-vessel molten corium in existing pressurized water reactors (PWR) and BWR plants without significant modification and costs. Experimental and modeling efforts were made to prove the feasibility of the proposed concept. Both bench-scale and large-scale experiments using a corium surrogate (lead oxide) demonstrated that the endothermic decomposition of a granular carbonate material upon interaction with molten oxide can effectively cool and therefore solidify the melt. to the experiments show that an open porous structure is formed that can also promote cooling. To model this dynamic process of SM-molten corium interactions, we began development of a detailed multi-physics model using a finite element code, with the eventual goal of helping to guide future bench-scale experiments, as well as linking this model to MELCOR. As an interim approach until the detailed model is completed, we developed a simplified shrinking core model. This shrinking core model was then used in MELCOR simulations to test the feasibility of using this injectable SM system in a realistic reactor environment.

Using MELCOR, we first simulated the FARO L26s corium spreading experiment with and without the carbonate SM. These simulations showed that the SM was effective in stopping the advance of the corium melt compared to scenarios where the SM was not present. The final corium spreading distance is a strong function of the particle size, as expected in the shrinking-core model since larger particles have lower surface area to volume ratios. On the other hand, a sensitivity study showed that the thermal conductivity, porosity of the carbonate bed, and CO_2 diffusivity have little influence on the cooling rate or stopping distance.

We implemented the same SCM model into a Mark I BWR-4 LTSBO MELCOR deck. Using 280 metric tons of the $CaCO_3$ for this simulation, the SM delays the severity of the accident and delays containment breach by 15 hours with the uncertainty of the 3 hours for the unreacted carbonate SMs. This additional time may allow remediation of the accident or allow extra time for evacuation of the workers and the public in the vicinity of the plant. Because the accident simulated had a leaking containment, the effect of this added gas pressure did not influence the containment pressure. Note that the containment temperature is lower with the carbonate SM than without it. This might also affect the final pressure of the containment. In addition, the possibility of a

hydrogen explosion could be minimized with the addition of the CO_2 by reducing the mole fraction of the hydrogen from the possible threshold for detonations. This will also decrease the severity of the accident. As a final note, MELCOR can be used to examine any new safety system through simulations such as the IMS without modifying the source code using control functions via inputs.

ACKNOWLEDGMENTS

This paper describes objective technical results and analysis. Any subjective views or opinions that might be expressed in the paper do not necessarily represent the views of the U.S. Department of Energy or the United States Government. Sandia National Laboratories is managed and operated by National Technology and Engineering Solutions of Sandia, LLC for U.S. DOE/NNSA under contract DE-NA0003525. This research was supported by the Laboratory Directed Research and Development Program of Sandia National Laboratories. The authors appreciated the FARO L-26S STRESA data from the Joint Research Centre, European Commission © Euratom, 2019. The authors also appreciated the peer review of this paper done by Lisa Mondy and previously by K.C. Wagner of Sandia and X-ray CT data provided by Dr. Anne Grillet.

REFERENCES

[1] Sappok, M. and Steinwarz, W., 1998. “COMAS Experiments as Contribution to the Validation of the EPR Mitigation Concept for Core Melt Accidents,” 6th International Conference on Nuclear Engineering (ICONE-6), San Diego, California, May 10-15.

[2] Magallon, D. and Tromm, W., 1999. “Dry and Wet Spreading Experiments with Prototypic Material at the FARO Facility,” OECD Workshop on Ex-Vessel Debris Coolability, Karlsruhe, Germany, November 15-18.

[3] Journeau, C., Boccaccio, E., Brayer, C., Cognet, G., Haquet, J .F., Jégou, C., Piluso, P. and Monerris, J., 2003. “Ex-Vessel Corium Spreading: Results from the VULCANO Spreading Tests,” Nuclear Engineering and Design, Vol. 223, pp. 75-102.

[4] Farmer, M.T., Sienicki, J. J. and Spencer, B. W., 1990. "The MELTSPREAD-1 Computer Code for the Analysis of Transient Spreading in Containments," ANS Winter Meeting Session on Thermal Hydraulics of Severe Accidents, Washington, DC, November 11-15.

[5] Suzuki, H., Matsumoto, T., Mitadera, T., Matsumoto, M., Sakaki, I., and Zama, T., 1993. “Fundamental Experiments and Analysis for Melt Spreading on a Concrete Floor,” 2nd International Conference on Nuclear Engineering (ICONE-2), San Francisco, CA, March 21-25.

[6] Piar, B., Michel, B. D., Babik, F., Latché, J. C., Guillard, G. and Ruggiéri, J. M., 1999. “CROCO: a Computer Code for Corium Spreading,” 9th International Topical Meeting on Nuclear Reactor Thermal Hydraulics (NURETH-9), San Francisco, California, October 3-8.

[7] Allelein, H. J., Breest, A. and Spengler, C., 1999. "Simulation of Core Melt Spreading with LAVA: Theoretical Background and Status of Validation," OECD Workshop on Ex-Vessel Debris Coolability, Karlsruhe, Germany, November 15-18.

[8] Spindler, B., Veteau, J. M., Brayer, C., Cranga, M., De Cecco, L., Montanelli, P. and Pineau, D., 1999. "Assessment of THEMA Code Against Spreading Experiments," OECD Workshop on Ex-Vessel Debris Coolability, Karlsruhe, Germany, November 15-18.

[9] Wittmaack, R., 1999. "Numerical Simulation of Corium Spreading in the EPR with CORFLOW," OECD Workshop on Ex-Vessel Debris Coolability, Karlsruhe, Germany, November 15-18.

[10] Veteau, M., Spindler, B. and Daum, G., 2003. "Modelling of Two-Phase Friction from Isothermal Spreading Experiments with Gas Fed from the Bottom and Application to Spreading Accompanied by Solidification," 10th International Topical Meeting on Nuclear Reactor Thermal Hydraulics (NURETH-10), Seoul, Korea.

[11] Dinh, T. N., Konovalikhin, M. and Sehgal, B. R., 2000. "Core Melt Spreading on a Reactor Containment Floor," Progress in Nuclear Energy, Vol. 36, pp. 405–468.

[12] Konovalikhin, M. J., 2001. Investigations on Melt Spreading and Coolability in a LWR Severe Accident, Ph.D. Thesis, Royal Institute of Technology, Stockholm, Sweden.

[13] Journeau ,C., Haquet, J., Spindler, B., Spengler, C. and Foit, J., 2006. "The VULCANO VE-U7 Corium Spreading Benchmark," Progress in Nuclear Energy, Vol. 48, pp. 215–234.

[14] Komley, S., Almjashev, V. I., Bechta, S.V., Khabensky, V.B., Granovsky, V. S., and Gusarov, V.V., 2015. "New Sacrificial Material for Ex-Vessel Core Catcher," Journal Nuclear Materials, 467, pg. 778-784.

[15] Farmer, M.T., 2009. Melt Spreading Code Assessment, Modifications, and Applications to the EPR Core Catcher Design, ANL-9/10, Argonne National Laboratory.

[16] Pikkarainen, M., Laine, J., Purhonen, H., Kyrki-Rajamaki, R., and Sairanen, R., 2008. "Heat Transfer Analysis of the European Pressurized Water Reactor (EPR) Core Catcher Test Facility Volley, Proceedings of the International Youth Nuclear Congress 2008.

[17] Louie, D.L.Y., Wang, Y., Rao, R., Kucala, A., Kruichak, J., and Chavez, W., 2019.A New Method to Contain Molten Corium in Catastrophic Nuclear Reactor Accident, SAND2019-13133, Sandia National Laboratories.

[18] Louie, D.L.Y., Wang, Y., Rao, R., Kucala, and A., Kruichak, "Using Alkaline Carbonate to Mitigate Molten Corium in Severe Nuclear Reactor Accidents," Proceedings of ICAPP 2021, October 16-20, 2021.

[19] Stanmore, B.R. and Gilot, P., 2005. “Review-Calcination and Carbonation of Limestone During Thermal Cycling for CO2 Sequestration,” Fuel Processing Technology, **86** 1707-1743.

[20] Lee, J-T., et al., “Thermal Decomposition of Limestone in a Large-Scale Thermogravimetric Analyzer,” Thermochimica Acta, 213, 223-240, 1993

[21] Do, D.H., et al., “Determination of Reaction Coefficient, Thermal Conductivity and Pore Diffusivity in Decomposition of Limestone of Different Origin,” Proceedings of the World Congress on Engineering and Computer Science 2011 (WCECS 2011), Vol II, San Francisco, CA, October 19-21, 2011.

[22] Specht, E., et al., 1986. “Reaction, Pore Diffusion and Thermal Conduction Coefficients of Various Magnesites and their Influence on the Decomposition Time,” Technische Universitat Clausthal.

[23] Hills, A.W.D., 1968. “The Mechanism of the Thermal Decomposition of Calcium Carbonate,” Chemical Engineering Science, Vol 23, pg. 297-320.

[24] Mikulcic, H., Berg, E., Vujanovic, M., Priesching, P., Perkovic, L., Tatschl, R., and Duic, N., 2012. “Numerical Modeling of Calcination Reaction Mechanism for Cement Production,” Chemical Engineering Science, 69, pg. 607-615.

[25] Kucala, A., Rao, R., and Erickson, L., 2019. “A Computational Model for Molten Corium Spreading and Solidification,” Computers & Fluids, **178**, 15, pg.1-14.

[26] Humphries, L.L., Beeny, B.A., Gelbard, F., Louie, D.L., and Phillips, J., 2018. MELCOR Computer Code Manuals, Vol.1: Primer and Users’ Guide, Version 2.2.11932, SAND2018-13559 O, Sandia National Laboratories.

[27] Amidu, M.A., and Addad, Y., 2021 “The influence of the water ingression and melt eruption model on MELCOR code prediction of molten corium-concrete interaction in the APR-1400 reactor cavity,” Nuclear Engineering and Technology, httos://doi.org/10.1016/j.net.2021.09.036.

[28] Alsmeyer, H., and Tromm, W., 1999.The COMET Concept for Cooling Core Melts: Evaluation of the Experimental Studies and Use in the EPR, FZKA 6186, EXV-CSC (99)-D036, Institut fur Kern- und Energietechnik, Forschungszentrum Karsruhe GmbH, Karlsruhe.

[29] Silverii, R., Magallon, D., 1998. FARO LWR Program – Test L-26S Data Report, Technical Note No. I.98.229, EXC-CSC (98)-D007, Institute for Systems, Informatics and Safety, Joint Research Center, Ispra, Italy.

List of Figures

Table 1. Typical energy absorption values of alkaline carbonate and water [17]

Energy absorption medium*	Temp. (°C)	Cooling Value		
		kJ/mole	kJ/g	kJ/ml
H_2O: liquid to gas phase	100	40.66	2.26	2.26
$CaCO_3 \rightarrow CaO+CO_2$	825	179.17**	1.78	5.03
$MgCO_3 \rightarrow MgO+CO_2$	350	100.69	1.19	3.64
$FeCO_3 \rightarrow FeO+CO_2$	350	75.09	0.65	2.53

*ρ and Cp for H_2O, $MgCO_3$, $FeCO_3$, $CaCO_3$ are 1, 3.05, 3.90, 2.71 g/cc, 75.35, 75.51, 82.1 and 83.5 J/mol-°C.

**A range of values have been reported as high as 182 kJ/mole [18].

Table 2. Experimental data [25]

Test Condition	
Melt composition (wt%)	80 UO_2+20 ZrO_2
Melt mass, kg	160.4
Substrate	Stainless steel
Spreading sector	17º
SARCOFAGO initial temperature	Room
SARCOFAGO initial pressure	Atmospheric**

**Argon gas is being used.

Table 3. Experimental results [25]

Melt	
Discharge rate, liter/s	2.06
Spreading time, seconds	18
Spreading distance, m	1.13
Maximum height, m	0.135
Maximum flow rate, m/s	0.503
Plate	
Maximum surface temperature, K	1358.2
State	Intact

Table 4. Sensitivity study for SCM on postulated SMs to FARO L-26S

Case	Description	Results (spread length, m)
Base	No carbonate	1.1264
1	r_0=0.01m, ε=0.4, λ=7 W/m-K, α=0.0165	0.4270
1a	Same as Case 1, except ε=0.5	0.4364
1aa	Same as Case 1, except ε=0.8	0.4842
1b	Same as Case 1, except λ=1 W/m-K	0.4334
1c	Same as Case 1, except α=0.00825	0.4270
2	Same as Case 1, except r_0=0.005m	0.4011
2a	Same as Case 2, except λ=1 W/m-K, ε=0.35	0.3953
3	Same as Case 1, except r_0=0.015m	0.4532
3a	Same as Case 3, except λ=1 W/m-K, ε=0.45	0.4653
4	Same as Case 1, except r_0=0.075m	0.4131

4a	Same as Case 4, except ε=0.375, λ=1 W/m-K	1.1264

*This height is still manageable because the wall near the cup is 0.15 m high

Table 5. MELCOR calculations key event timing [17]

Event	Timing (hr:min:sec)	
	Without $CaCO_3$	With $CaCO_3$
Loss of all AC power	00:00:00	00:00:00
MSIVs close	00:00:00+	00:00:00+
SCRAM	00:00:00+	00:00:00+
RCIC starts on low level	00:10:19	00:10:19
Operators initiate 100 °F/hr (37.8 °C/hr) cooldown (SRV opened, RCIC throttled)	01:00:00	01:00:00
SRV closes on battery depletion	04:00:00	04:00:00
RCIC turbine floods failing RCIC	5:53:37	5:53:37
Downcomer level drops to TAF	8:29:52	8:29:52
First fuel-cladding gap release	9:31:39	9:31:39
Cycling SRV fails to reclose	NA	NA
MSL rupture	12:03:37	12:03:37
Drywell head flange leakage begins	12:04:12	12:04:12
Reactor building (refueling bay) blow-out panels blow out	12:05:08	12:05:08
First large-scale relocation of core debris to lower plenum	12:40:27	12:40:27
RPV lower head dry	13:10:54	13:10:54
RPV lower head failure	18:37:56	18:37:56
$CaCO_3$ reaction begins	NA	18:38:00
Core-concrete interaction begins	18:37:57	33:15:00
Drywell liner melt-through	19:46:21	37:37:54
$CaCO_3$ consumed	NA	34:05:00
H_2 burns initiate in reactor building grossly damaging the building	19:46:42	37:38:39

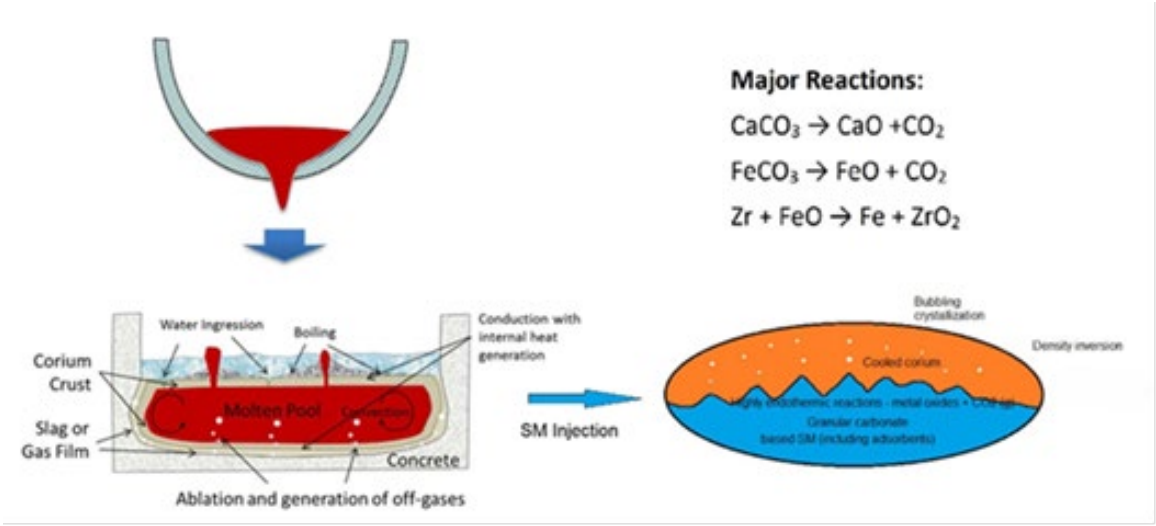

Figure 1. Possible reactions of molten corium with concrete in a cavity. As corium pours onto the cavity, the molten corium reacts with the concrete and water to create slag or gas film. As crust forms, water is boiling and trying to ingress into the corium crust. Possible SM injection as carbonate reactions as shown to cool and contained the corium.

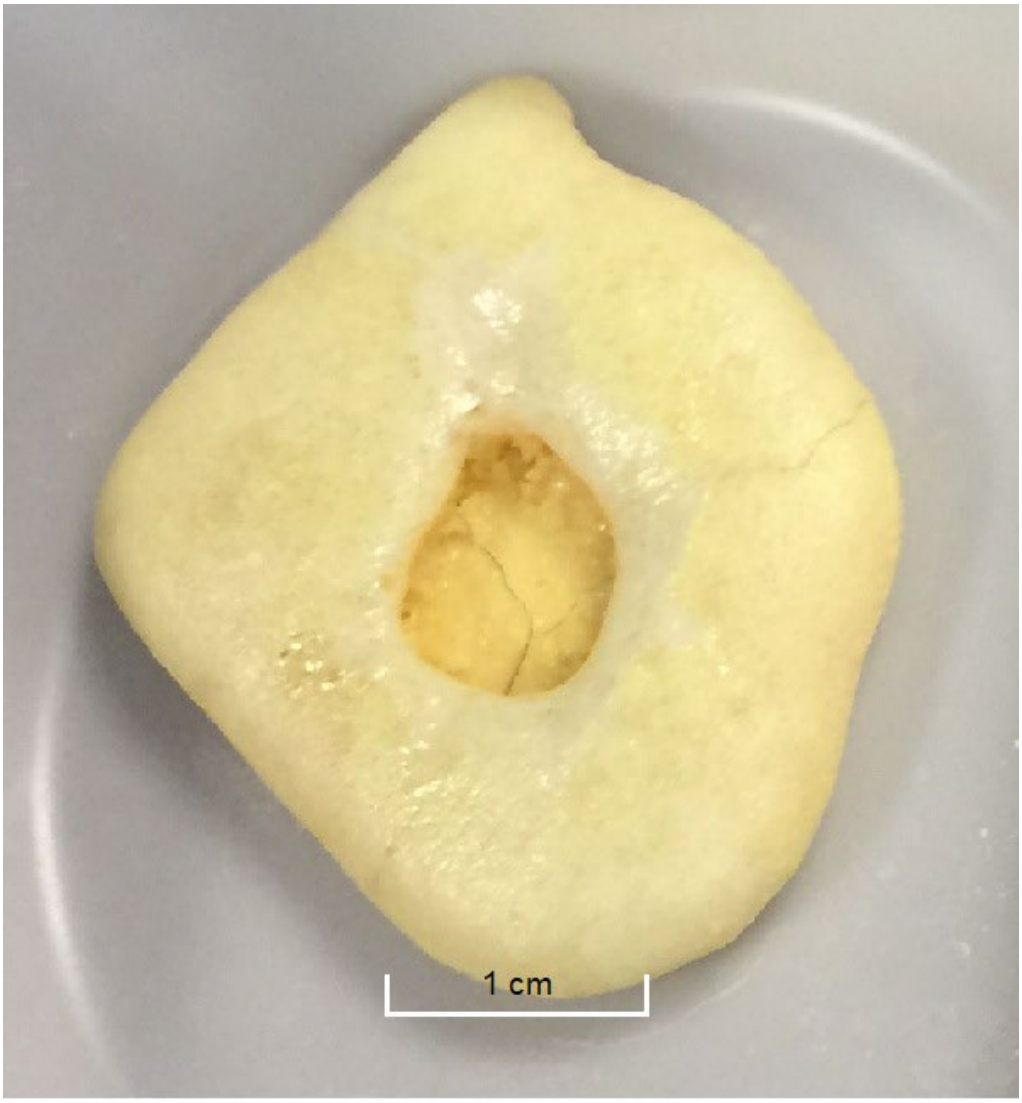

Figure 2. Small-scale Test Sample 1E used in the porosity determination. A small sample measuring 9.1 g ($CaCO_3$ powder) was preheated to 550 ºC in a petri dish. Final sample has a center hole is formed due to the CO_2 gas generated. Using a displacement method, the porosity is estimated to be 70%.

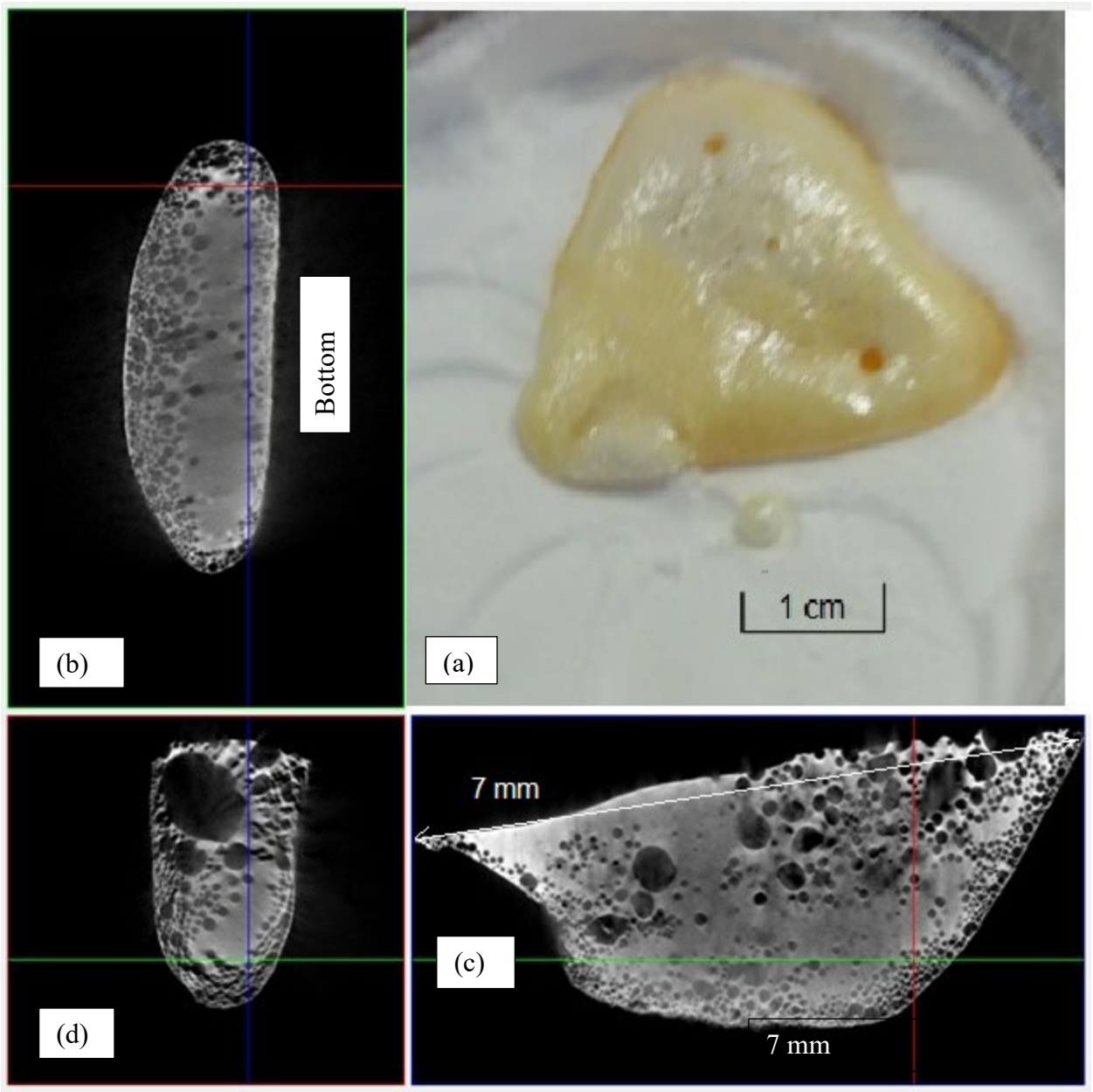

Figure 3. Small-scale Test Sample 4B with 23.8 g of CaCO3 powder was not preheated in a peri dish: (a) after pour and cool, (b) to (d) are the X-ray μCT imaging of the micro bubbles in the sample. (b) The bubbles were concentrated near the surfaces, with large bubbles near the top surface. (c) and (d) Additional evidence of bubble concentrated near the surface of sample.

Figure 4. Small scaled 5F Test sample (dolomite) at 23.5 g was not preheated in a peri dish after cool, showing evidence of convective flow of the dark granules that were noticeable concentrated on the surface of the sample.

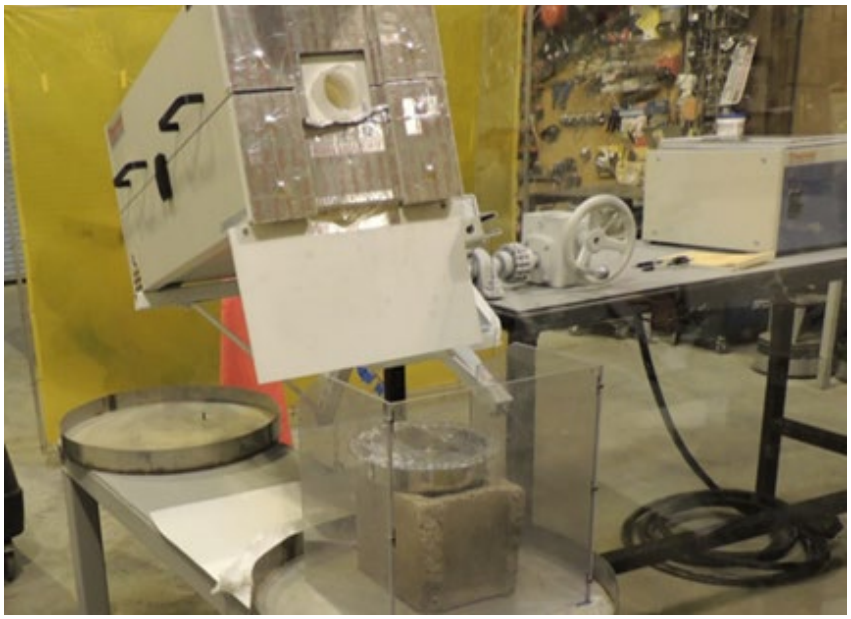

Figure 5. Apparatus of for studying SM-molten PbO interactions. A tube furnace is connected to a crank for pouring molten PbO onto a carbonate mineral bed in a catch pan.

(a) pour

(b) after cool

Figure 6. Large-scale Test 7 with 1.01 kg of PbO onto a bed of granular (< 1mm) calcites. (a) molten stream of PbO onto the pan containing calcites. (b) post-test configuration of the sample after cool with evidence of porous yellowish mixture of PbO and CaO.

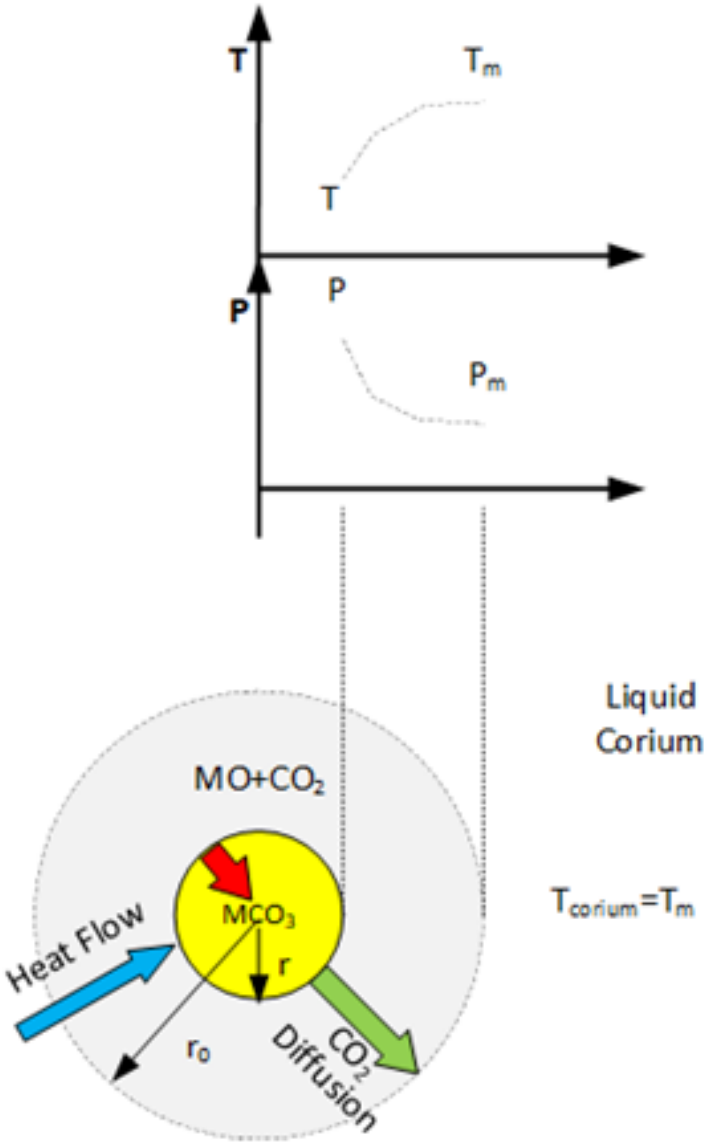

Figure 7. Simplified carbonate-corium equilibrium model.

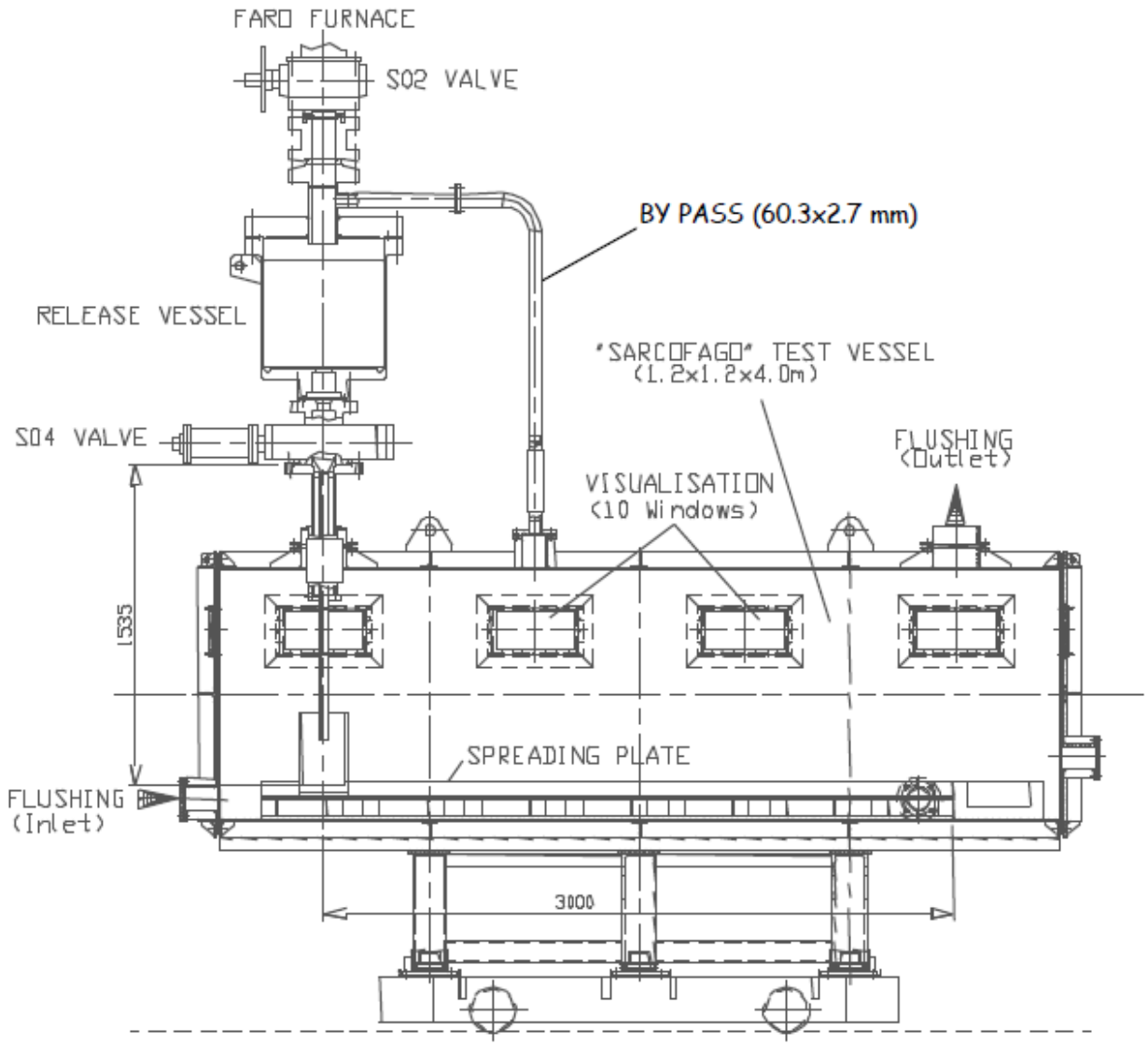

Figure 8. Layout of the SARCOFAGO vessel for FARO L-26S experiment [17].

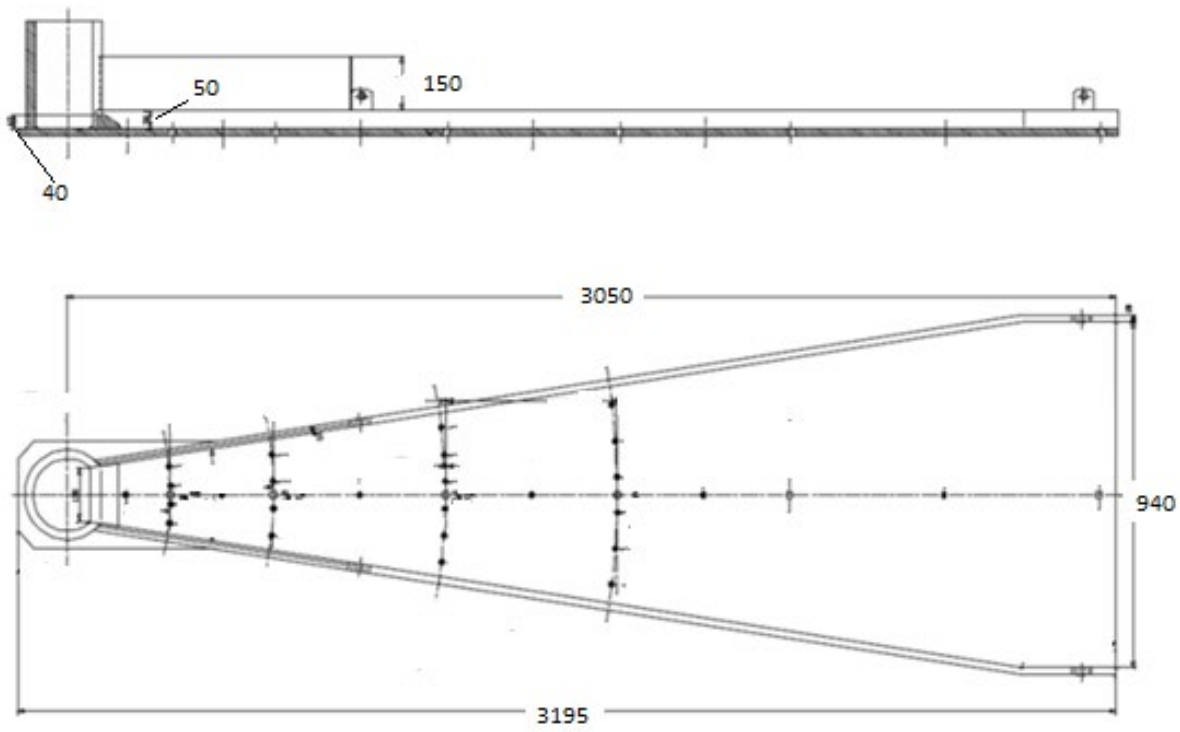

Figure 9. Spreading plate geometry (# in mm) [17].

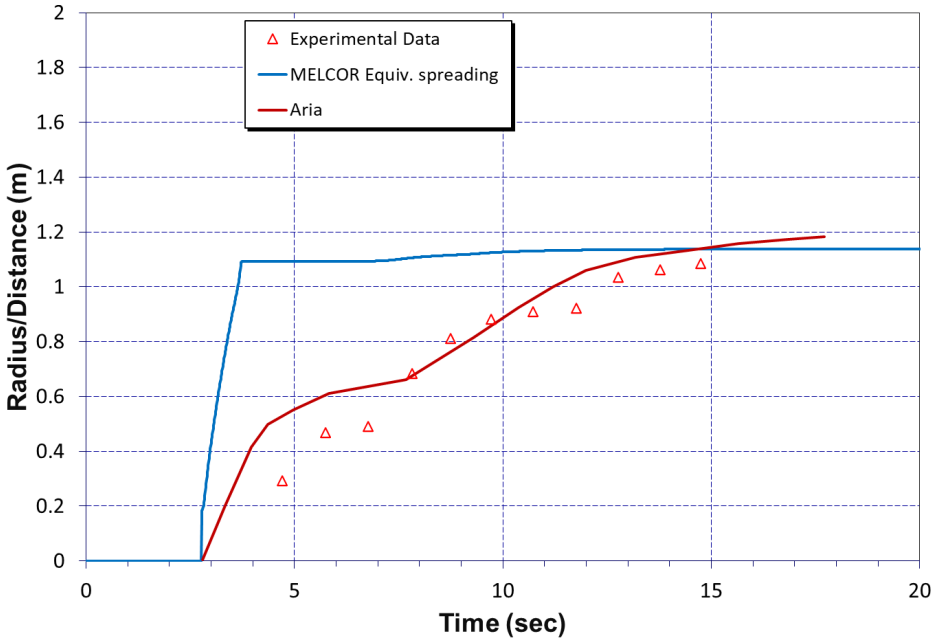

Figure 10. Comparison of the spreading distance of FARO L-26S experiment from MELCOR, Aria and experimental data.

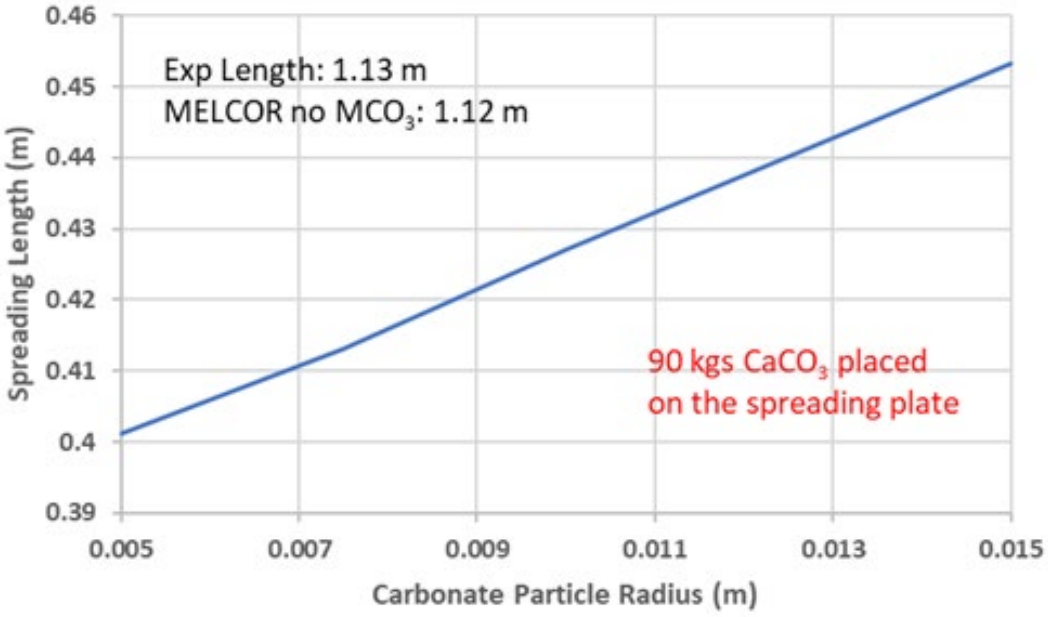

Figure 11. Spreading length as function of carbonate particle radius for L-26S, showing a confirmation of without using $CaCO_3$ to absorb the melt's heat (MELCOR yielded 1.12 m with experiment data of 1.13 m. A 90 kg of $CaCO_3$ underneath the melt would reduce spreading length to ~ 0.45 m

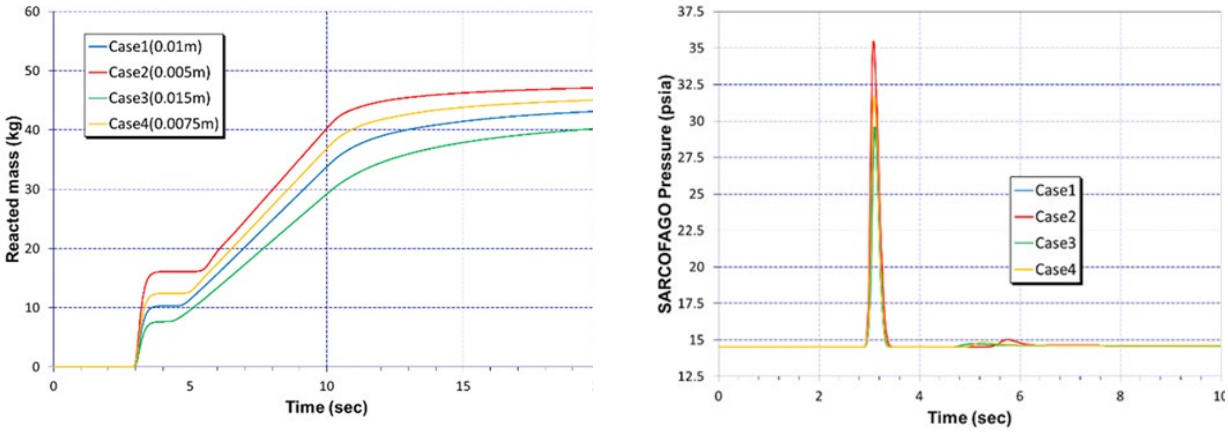

(a) Carbonate Reacted Mass (b) Gas Pressure

Figure 12. Sensitivity study on carbonate reacted mass and pressure results for the L-26S geometry as a function of particle size. The pressure rise is proportional to the reacted mass. (a) the carbonate size effect on the amount of reacted mass. The size of 0.005 m yielded the most reacted mass. (b) corresponding pressure for the cases in (a). The pressure rise is proportional to the reacted mass.

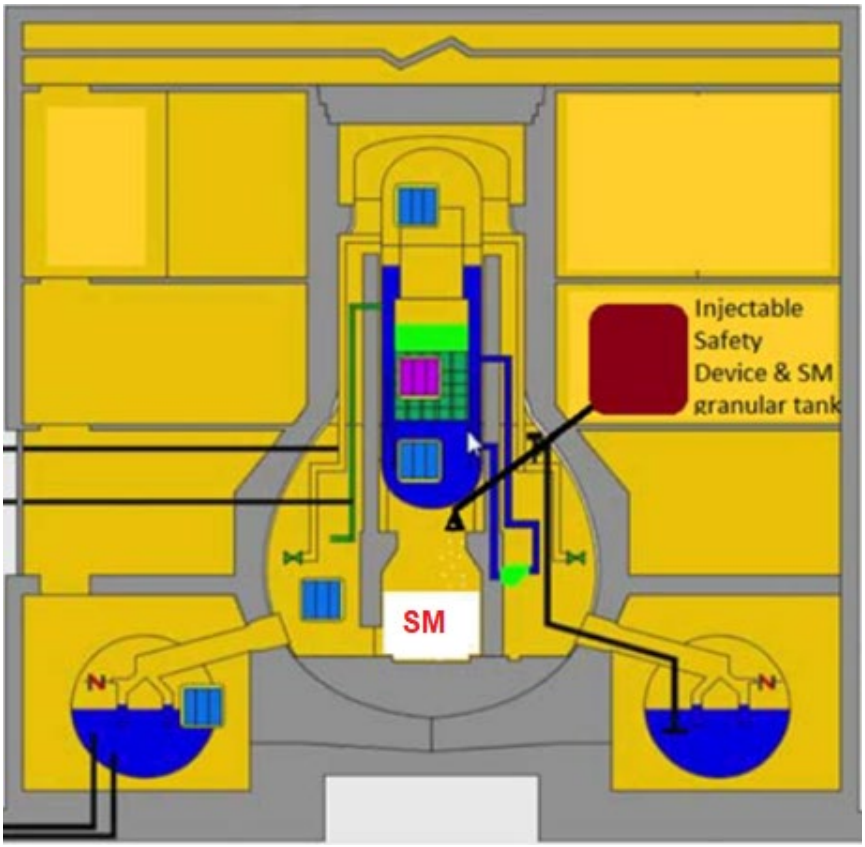

Figure 13. Schematic of implementing an injectable safety device and location of granular SM ($CaCO_3$) tank in Mark I containment. The granular SM needs to be placed underneath the RPV so when it breaches, the molten corium will fall onto the SM bed.

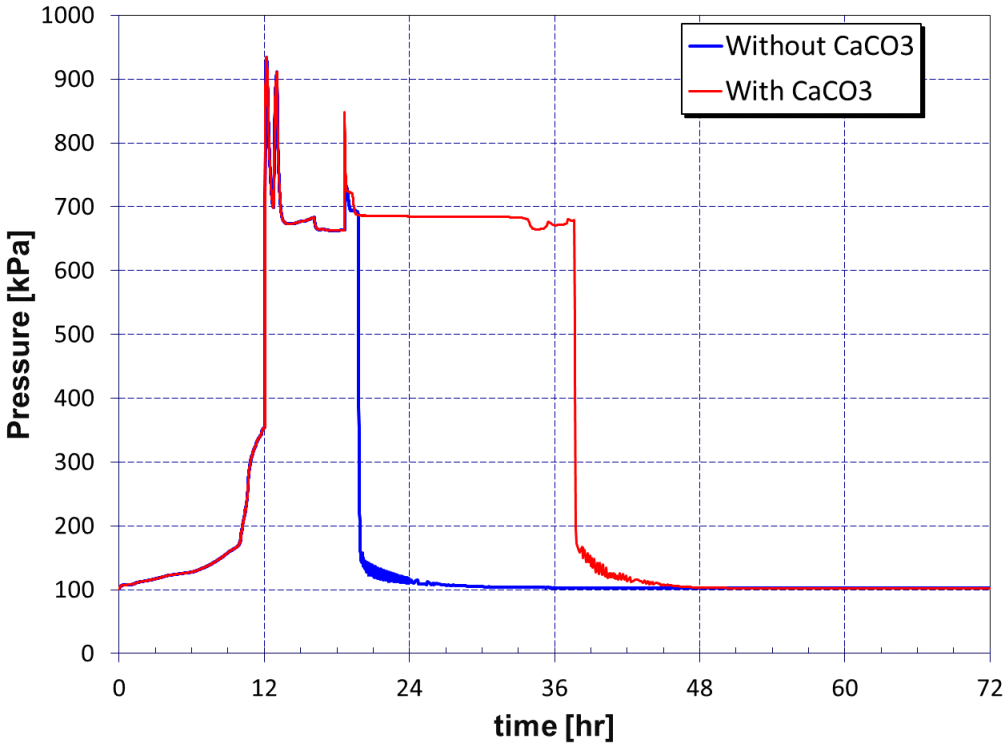

Figure 14. MELCOR simulation results: containment pressure comparison with and without $CaCO_3$ for Mark I BWR, showing the delay of the containment failure with the use of $CaCO_3$.

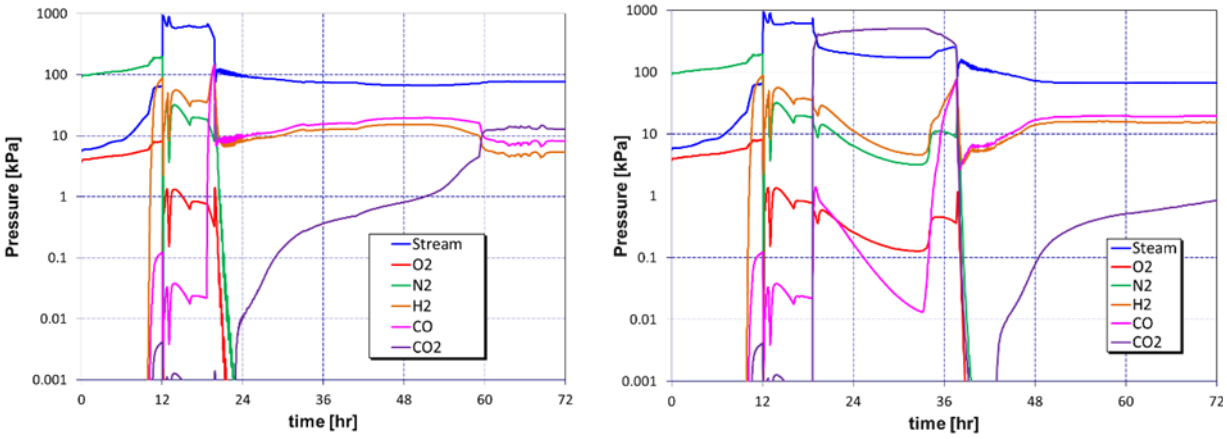

(a) Without $CaCO_3$ (b) With $CaCO_3$

Figure 15. MELCOR simulation results: Mark I BWR containment partial pressure without and with $CaCO_3$. (a) the partial pressures of gases for the case without $CaCO_3$. (b) the partial pressures of gases for the case with $CaCO_3$.

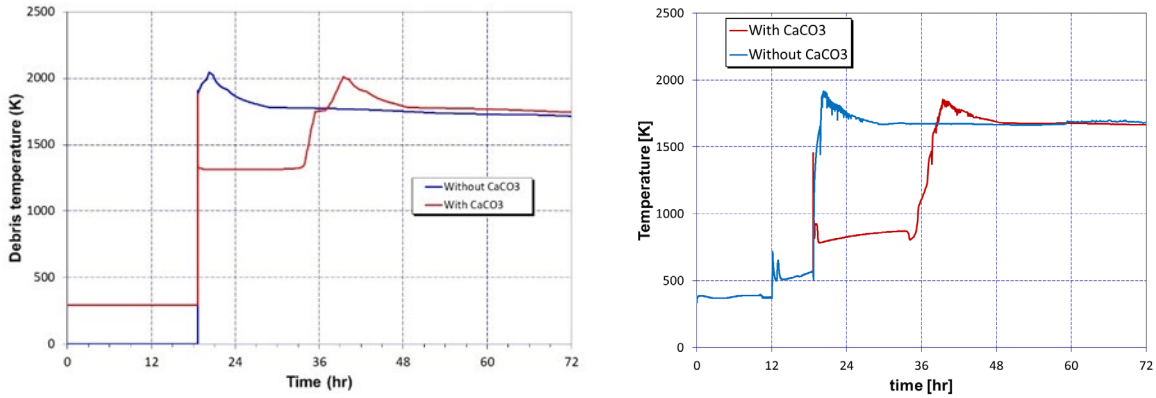

(a) Debris (b) Gas volume

Figure 16. MELCOR simulation results: Mark I BWR pedestal debris and gas temperature comparison of the cases with and without $CaCO_3$. (a) debris temperatures showing the case with $CaCO_3$ yielded a lower debris temperature. (b) pedestal gas temperature showing the case with CaCO3 yielded a lower gas temperature.

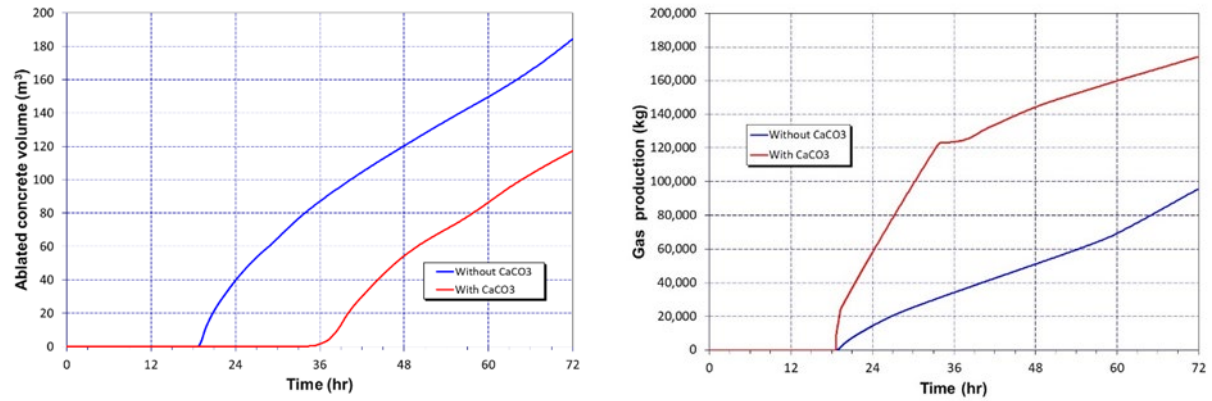

(a) Ablation concrete volume (b) Integral gas release from decomposition and ablation

Figure 17. MELCOR simulation results: Mark I BWR ablated concrete volume and integral gas release comparisons with and without $CaCO_3$. (a) concrete ablation volume decreased for the case with $CaCO_3$. (b) gas production increases with the case of CaCO3 which were from the decomposition and ablation.

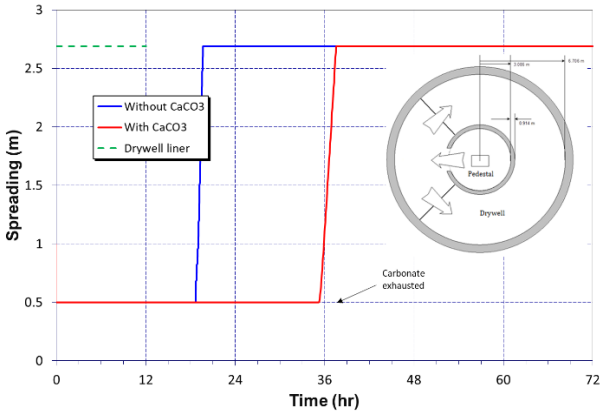

Figure 18. MELCOR simulation results: Mark I BWR debris spreading on containment floor from pedestal toward drywell liner comparison of cases with and without $CaCO_3$. The case with $CaCO_3$ yielded a delay time to reach to the drywell liner.

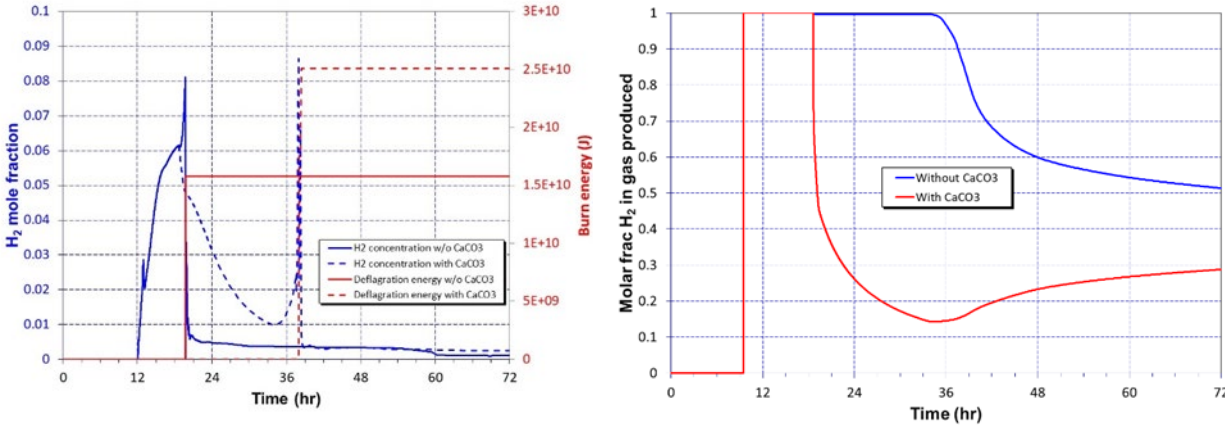

(a) Refueling Bay H_2 concentration/burn energy

(c) H_2 molar fraction produced

Figure 19. MELCOR simulation results: Mark I BWR refueling bay H_2 concentration and burn energy, and H_2 molar fraction produced comparison for cases with and without $CaCO_3$. (a) Refueling Bay H_2 concentration/burn energy. (b) H_2 molar fraction produced.